PAPER

Thermo- and oxidation-sensitive poly(meth) acrylates based on alkyl sulfoxides: dual-responsive homopolymers from one functional group†

Doğuş Işık,[a] Elisa Quaas[b] and Daniel Klinger [ID] *[a]

Ideal dual-responsive homopolymers are derived from monomers that unite two sensitive functionalities in one molecule. This design circumvents structural inhomogeneities that can occur during the preparation of similar copolymers from two different monomers. Among such "smart" homopolymers, materials that sense changes in temperature and redox activity are of special interest due to the ubiquitous availability and facile applicability of both stimuli. However, developing new monomers that combine both response mechanisms in one functional motif remains challenging. To address this challenge, we introduce a new class of (meth)acrylates bearing alkyl sulfoxide side groups to realize thermo- and oxidation-responsive homopolymers. The dual-responsive behavior follows specific design principles: first, the thermo-responsive behavior can be tuned by balancing sulfoxide-water hydrogen bonds and hydrophobic interactions of the respective alkyl side chains. Following this molecular design, we found that systematically varying the sulfoxides' alkyl groups can be used to tune the thermo-responsive properties of the polymers. Second, an additional oxidation response is introduced by oxidizing the hydrophilic sulfoxides to their hydrophobic sulfone analogues. This decreases the polymer's overall hydrophilicity, thus reducing the cloud point temperature. As a result, the polymer exhibits a dual-responsive behavior. In addition, the gradual partial oxidation of sulfoxides gives the advantage to adjust the thermo-responsive profile though the second stimulus. We believe that this unique combination of thermal and oxidation response in one single functional unit, its facile synthesis, well-controlled polymerization, and biocompatibility is the starting point for the preparation of highly sophisticated materials for a wide variety of applications.

Introduction

Nature is able to control highly complex functions by precisely adapting macromolecular properties to multiple environmental changes. To mimic such outstanding biological versatility with "smart" synthetic polymers, different functional moieties need to be combined within one polymer chain.[1–3] The resulting dual- or multi-responsive polymers enable new levels of materials' variability and complexity, and are paving the way to new advanced applications.[4–6]

Among such emerging dual-stimuli-responsive materials, (water soluble) polymers that sense changes in temperature

and redox-activity are of special interest for applications in the biomedical field,[7,8] information processing,[9] and nanotechnology.[10,11] This can be attributed to the ubiquitous availability and efficient applicability of both stimuli in different environments. In addition, the orthogonal sensitivity to temperature as physical trigger and redox active reagents, such as reactive oxygen species (ROS), as chemical oxidation trigger gives rise to innovative smart materials with non-interfering dual functions.[12,13]

While a plethora of polymers have been developed to exhibit either a thermo- or oxidation-response individually, examples that combine both properties in one dual-responsive-polymer are still limited. Existing multi-sensitive polymers have been realized mainly by (controlled) radical copolymerization of thermo- and oxidation-responsive monomers[14,15] or by step growth polymerization *i.e.* of poly(ethylene glycol) diacrylate with bridging thioether groups.[16] Even though such random copolymerization strategies are synthetically easy to realize, the concerted distribution of both stimuli-sensitive

[a]*Institute of Pharmacy, Freie Universität Berlin, Königin-Luise-Straße 2-4, 14195 Berlin, Germany. E-mail: daniel.klinger@fu-berlin.de*
[b]*Institute of Chemistry, Freie Universität Berlin, Takustraße 3, 14195 Berlin, Germany*
†Electronic supplementary information (ESI) available. See DOI: 10.1039/d0py01321h

groups along the same backbone can significantly affect the individual response profiles.[17–20] In case of step growth polymerizations, this approach often leads to broad molecular weight distributions restricts the access to well-defined (block) copolymer structures. Overall, the co-dependency between two monomers along one backbone as well as the distribution of functional moieties in the backbone and side chains can limit the synthetic flexibility and hinders the facile adjustment of accurate transition temperatures.[14,20–22]

To overcome such copolymerization disadvantages, new strategies aim to combine two different responsive groups in one multi-stimuli-responsive monomer.[23–25] The resulting homopolymers allow accurate multi-stimuli-responsive profiles that do not depend on copolymer compositions.[26,27] However, the synthetic introduction of multiple functional groups in one monomer is far from trivial and such strategies are, until now, mainly reported for combinations of temperature with light and/or pH.[28–30] For example, monomers containing *meth*acrylamides and aspartic acid groups were designed to exhibit temperature response due to the acrylamide groups and pH response due to the carboxylic acid groups.[31] Difficulties of this approach stem from the large multi-functional monomers which can hinder efficient and controlled polymerization.[14,23] In addition, the close spatial proximity of the sensitive groups can further influence the response behavior of each other.[32,33]

Hence, ideal multi-responsive polymers reduce the complexity of the macromolecular design even further: in such advantageous systems, monomers contain only one functional group that can respond to both stimuli.[25] A prominent example of this approach is poly[*N*-[2-(diethylamino)ethyl] acrylamide] (pDEAEAm) where the dimethylamino group is responsive to both temperature and pH (and CO_2) changes.[34] For polymers that respond to temperature and oxidative species, such a design would also allow for the precise adjustment of a cooperative stimuli-response profile. Here, the response to one trigger (temperature) can be adjusted through the application of the second stimulus (oxidation). The resulting dual-responsive homopolymers enable to examine and apply structure–property-relations much more precisely than similar copolymer systems. While such multi-responsive functional groups are a promising concept, an actual simple molecular design and straightforward synthesis of thermo- and oxidation-responsive monomers is still very challenging.

To address this challenge, we have considered two important criteria for a respective molecular design: first, the polymers' thermo-responsive behavior depends on a specific balance between polymer–water hydrogen bonds and intra-/inter-polymer hydrophobic interactions. Hence, the respective monomers are inherently amphiphilic and the balance between hydrophilic hydrogen bonds and hydrophobic groups determines the thermo-responsive profile.[35] Second, introducing an additional oxidation response requires this thermo-responsive monomer to change its amphiphilicity upon oxidation. This can be realized if the hydrophilic group is oxidized to a more hydrophobic state with less hydrogen bonds.

As a result, the hydrophilic-to-hydrophobic ratio of the thermo-responsive polymer is lowered and the polymer–water hydrogen bonds will be reduced. This will cause the cloud point temperature to decrease and the polymer will thus exhibit a multi-responsive behavior.
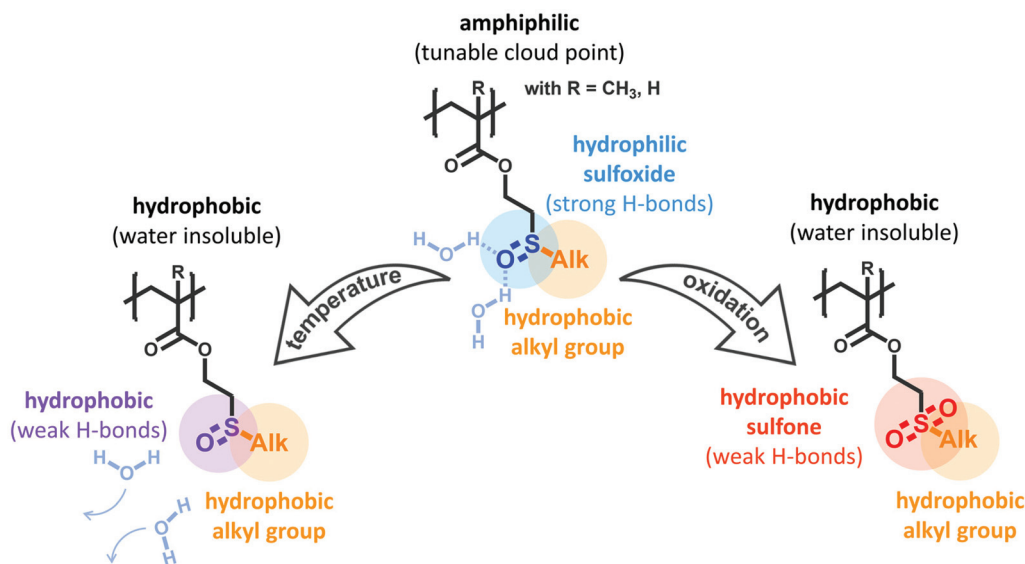
We found sulfoxide groups to meet these requirements perfectly. First, they are strong hydrogen bond acceptors and are therefore very hydrophilic.[36,37] In polymers, side-chain sulfoxide poly(meth)acrylates are known for their very low cytotoxicity, their excellent biocompatibility, and their penetration enhancing features with potential applications in pharmaceutical and medical sciences.[38–40] Due to this strong inherent hydrophilicity, polysulfoxides were also proposed to have active "stealth" properties similarly to polyethylene glycol (PEG).[41] Second, when sulfoxides are oxidized to the corresponding sulfones, the ability to form hydrogen bonds with water is dramatically reduced. Since this oxidation of sulfoxide-containing polymers can occur effectively as response to reactive oxygen species (ROS), polymers containing sulfoxide side groups show great potential for realizing oxidation-responsive materials.[41,42]

Based on these considerations, we herein report the rational design of new alkyl sulfoxide containing (meth)acrylates as monomers for thermo- and oxidation-responsive polymers (see Scheme 1). In these monomers, the central role of the sulfoxides is twofold: on one hand, the strong hydrogen bond acceptors will be combined with hydrophobic alkyl side groups to realize an amphiphilic structure. This is the foundation for thermo-responsive polymer properties. Here, the cloud point temperature can easily be tuned by varying the alkyl side chain, *i.e.* the hydrophilic-to-hydrophobic balance of the monomer. On the other hand, oxidation of the sulfoxides to the respective sulfones will reduce the polymers' hydrophilicity. Thus, a quantitative oxidation results in a dramatically reduced water solubility. In addition, the oxidation-sensitive behavior also offers the potential to gradually adjust the thermo-responsive profile. By controlling the conversion of sulfoxide to sulfone side groups, the cloud point temperature can be continuously decreased with an increasing number of sulfones per polymer.

We believe that this unique combination of the thermal and oxidation response in one single functional unit, it's facile synthesis, and well-controlled polymerization is the starting point for the preparation of highly sophisticated materials for a wide variety of applications.

Results and discussion

For the development of a sulfoxide-based thermo- and oxidation-responsive polymer, several steps need to be addressed. First, suitable functional groups have to be identified and incorporated into the monomer structure in a facile and efficient way. Second, a suitable polymerization method has to be chosen to give polymers with well-defined molecular weights and narrow molecular weight distributions. By doing

amphiphilic
(tunable cloud point)

with R = CH₃, H

hydrophilic sulfoxide (strong H-bonds)

hydrophobic (water insoluble)

hydrophobic alkyl group

hydrophobic (water insoluble)

hydrophobic (weak H-bonds)

hydrophobic alkyl group

hydrophobic sulfone (weak H-bonds)

hydrophobic alkyl group

temperature

oxidation

Scheme 1 Sulfoxide side groups as thermo- and oxidation-responsive motifs. Temperature-sensitivity is based on reducing the amphiphilic balance between hydrophilic sulfoxide moieties and hydrophobic alkyl groups at elevated temperatures. A second oxidative trigger turns the sulfoxide moieties into the respective hydrophobic sulfone derivatives, thus reducing polymer solubility and realizing a dual-responsive system.

so, a high degree of comparability is ensured that would enable to accurately determine the structure–property relationships. Third, the polymers should maintain their structural and functional integrity throughout the synthesis to preserve both the thermal und oxidation response. Addressing these challenges allows for an accurate and systematic investigation of a dual-stimuli-responsive polymer library.

**Preparation of an amphiphilic sulfoxide polymer library**

Key to the rational macromolecular design in this work is the combination of hydrophilic and oxidation-responsive sulfoxide moieties with different hydrophobic alkyl groups (see Scheme 1). The resulting amphiphilic structure is generally regarded as a main requisite for the introduction of thermo-responsive polymer properties such as a lower critical solution temperature (LCST). Here, it is assumed that the cloud point temperature (T_{cp}) can easily be tuned by varying the hydrophobic contribution of the alkyl side group, *i.e.* larger alkyl side groups would decrease the T_{cp}. Additionally, the polymer backbone itself can alter the hydrophilic-to-hydrophobic balance of the polymer. In general, a polyacrylate backbone is less hydrophobic than its poly*meth*acrylate analogue. This implies that the T_{cp} of polyacrylates would increase with respect to comparable poly*meth*acrylates. To analyze these two structure–property-relations systematically, a library of sulfoxide-containing poly*meth*acrylates and polyacrylates with varying alkyl side groups was investigated (Fig. 1a).

Monomer synthesis. To realize this polymer library, the following functional monomers were synthesized and denoted as follows: 2-(*alkyl*-**s**ulfoxide)**e**thyl *meth*acrylates (*alkyl*-**SEMA**) with methyl (Me), ethyl (Et), isopropyl (iPr), *n*-propyl (*n*Pr) and, *n*-butyl (*n*Bu) as alkyl groups and 2-(*alkyl*-**s**ulfoxide)**e**thyl **a**cry-

lates (*alkyl*-**SEA**) with isopropyl (iPr), *n*-propyl (*n*Pr), *n*-butyl (*n*Bu) as alkyl groups, respectively. Each monomer was synthesized *via* a two-step reaction route. For this, 2-thioethanol reagents with different alkyl substituents were reacted first with (meth)acryloyl chloride under basic conditions *via* a simple nucleophilic addition and elimination reaction. The intermediate products, 2-(Me, Et, iPr, *n*-Pr, *n*-Bu-thio)ethyl (meth)acrylates, were isolated and then reacted with *meta*-chloroperbenzoic acid (*m*CPBA). This facile, fast, and efficient oxidation reaction affords the targeted alkyl sulfoxide (meth)acrylate monomer library in good yields (see ESI section I† for further experimental details and characterization).

Polymer synthesis. Having demonstrated a straight-forward synthesis for the monomers a suitable polymerization technique is required. As mentioned above, it is critical to prepare polymers with comparable architectures (DP, size distribution) to ensure direct comparability between polymer structure and its responsive functions. To meet these synthetic requirements, reversible addition–fragmentation chain transfer (RAFT) radical polymerization was chosen. It is a highly powerful synthetic tool due to its versatility with respect to reaction conditions, functional group tolerance, and suitable monomer classes.[43,44] Using this controlled radical polymerization technique, functional alkyl sulfoxide-containing homopolymers with well-defined molecular weights and narrow molecular weight distributions were prepared. The RAFT solution homopolymerization of the alkyl sulfoxide *meth*acrylate monomer library was performed using cumyl dithiobenzoate (CDTB) as a chain transfer agent (CTA), AIBN as a radical initiator, and DMF as solvent with an initial feed ratio of $[\text{monomer}]_0 : [\text{CDTB}]_0 : [\text{AIBN}]_0 = 150 : 1 : 0.125$ (Table 1), thus targeting a DP of 150 for all polymers. As shown in Table 1,
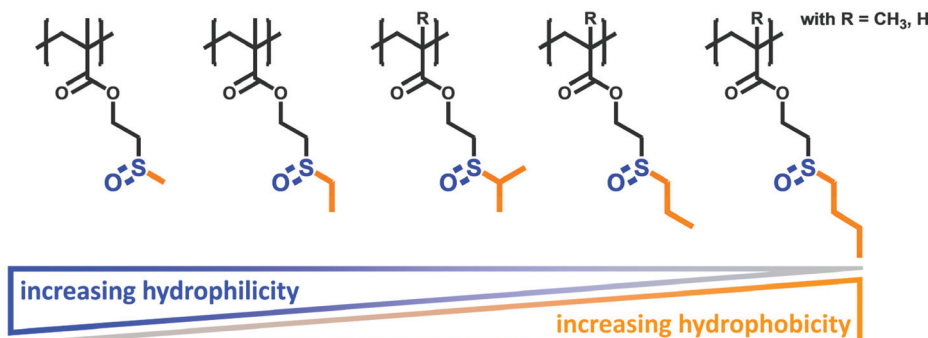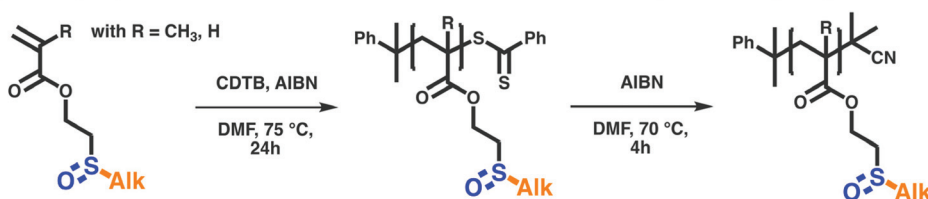
Fig. 1 (a) The investigated library of alkyl sulfoxide (meth)acrylate polymers. Varying the polymer's amphiphilicity by changing the alkyl group and the polymer backbone gives access to analyzing the structure–property relations of the thermo-responsive polymers. (b) Polymer synthesis was achieved *via* RAFT polymerization with subsequent end group removal.

Table 1 RAFT homopolymerization shows good control over DP and dispersity of *meth*acrylate monomers Me-SEMA, Et-SEMA, iPr-SEMA, *n*Pr-SEMA, *n*Bu-SEMA. Reactions were performed in DMF ([M] = 1 M) with [M] : [CDTB] : [I] = 150 : 1 : 0.125 at 75 °C for a reaction time of 24 h. Accounting for the lower conversion of the acrylate monomers iPr-SEA, *n*Pr-SEA and *n*Bu-SEA, the respective RAFT polymerizations were performed in dioxane ([M] = 1 M) with [M] : [BBDT] : [I] = 250 : 1 : 0.125 at 75 °C for a reaction time of 24 h

Polymer	CTA	[M]/[CTA]	Conv.[a] (%)	$M_{n,target}$ (g mol^{-1})	$M_{n,NMR}$ (g mol^{-1})	DP	$M_{n,GPC}$[b] (g mol^{-1})	$Đ$[b]
P(Me-SEMA)	CDTB	150	84	26 430	22 100	124	20 100	1.24
P(Et-SEMA)	CDTB	150	92	28 540	26 200	136	19 900	1.24
P(iPr-SEMA)	CDTB	150	86	30 640	26 500	128	23 200	1.20
P(*n*Pr-SEMA)	CDTB	150	88	30 640	26 900	130	22 400	1.21
P(*n*Bu-SEMA)	CDTB	150	95	32 750	31 000	141	22 400	1.19
P(iPr-SEA)	BBDT	250	51	47 600	24 400	127	19 200	1.31
P(*n*Pr-SEA)	BBDT	250	50	47 600	23 800	124	18 900	1.33
P(*n*Bu-SEA)	BBDT	250	48	51 100	24 600	119	15 300	1.29

[a] Conversion measured by ^{1}H NMR spectroscopy. [b] DMF LiBr (10 mM) eluent, linear PMMA standard.

the RAFT method gave good control over the polymerization process for the *meth*acrylate monomers. High conversions were reached and overall narrow molecular weight distributions ($Đ \leq 1.25$) were obtained.

Furthermore, the RAFT solution homopolymerization of the alkyl sulfoxide acrylate monomers was initially performed using the same reaction conditions as for the *meth*acrylates (CDTB, AIBN, DMF with $[monomer]_0 : [CDTB]_0 : [AIBN]_0 = 150 : 1 : 0.125$). However, under these conditions only lower molecular weight polymers were obtained (see ESI section II, Table S1†). To address this observed lower conversion for the acrylate monomers different dithioester and trithiocarbonate CTA's, namely benzyl benzodithioate (BBDT), 4-cyano-4-(thio-benzoylthio)pentanoic acid, dibenzyltrithiocarbonate, 4-cyano-

4-ethyl-trithiopentanoic acid, 4-cyano-4-dodecyl-trithiopenta-noic acid and 2-(((butylthio)carbonothioyl)thio)-2-methyl-propanoic acid were investigated. Unfortunately, for the majority of these CTAs either small molecular weights or high molecular weight dispersities were determined by GPC (data not shown). However, benzyl benzodithioate (BBDT) showed acceptable dispersities even though the molecular weight was lower than expected. This stems from the lower conversions in comparison to the poly*meth*acrylates thus indicating a slower polymerization process.

Taking these finding into account, we aimed to prepare polyacrylates with higher molecular weights. For this, BBDT in dioxane was used with an initial [M]/[CTA] = 250 to account for the slow polymerization and the corresponding low conver-

sion. Under these polymerization conditions, polyacrylates with degrees of polymerization comparable to the poly*meth*acrylates with [M]/[CTA] = 150 were obtained with reasonable dispersities (*Đ* ≤ 1.33) (Table 1). The DP and molecular weights ($M_{n,NMR}$) of all RAFT polymers were calculated by ^{1}H NMR spectroscopy (for details see ESI section III†).

After polymerization, the final alkyl sulfoxide-containing polymers were prepared by removal of the RAFT end group. This was necessary since the labile dithioester end groups might cause undesired side effects in upcoming polymer property measurements.[45] To prevent this, the CTA of the macromolecules was cleaved *via* a radical substitution reaction with AIBN. This introduces a more robust dimethyl nitril group (Fig. 1b).

Once having obtained a library of sulfoxide-containing homopolymers, the respective polymer analogues with sulfone side groups were prepared as controls. In these polymers, the central role of the alkyl sulfones is as follows: regarding temperature-responsive properties, the sulfones are inherently hydrophobic with no ability to form strong hydrogen bonds. Thus, in combination with the alkyl side groups, this results in an overall hydrophobic polymer with no potential to show temperature-responsive solution properties. This is in direct contrast, to the amphiphilic sulfoxides where thermo-responsive polymer properties are easily tuned *via* changing the hydrophilic-to-hydrophobic balance. Regarding the oxidation-responsive mechanism, the quantitative oxidation of the sulfoxides to the respective sulfones is the endpoint of this reaction. Thus, the hydrophobic sulfone polymers act as the control group for the assessment of the special thermo- and oxidation-responsive properties of the sulfoxide polymers. To ensure comparability (same DP and *Đ*) between sulfoxide and sulfone polymers, a complementary library of sulfone (meth) acrylate polymers was prepared by simple oxidation of the previously prepared sulfoxide polymers (see ESI section IV† for further experimental details and characterization).

Screening of the thermo-responsive properties of the sulfoxide- and sulfone-containing polymers

Having established a straightforward synthetic route to prepare a functional library of comparable sulfoxide- and sulfone-containing (meth)acrylate polymers, their temperature-dependent solution properties were assessed. As mentioned in the previous section, it is assumed that the cloud point temperature (T_{cp}) decreases with longer alkyl groups. As shown in Fig. 2a, an initial screening of the solubility revealed that only polymers with alkyl side groups up to 3 carbons (Me to iPr or *n*Pr) were water soluble at room temperature. The butyl sulfoxide-based poly*meth*acrylate was completely insoluble in water and the polyacrylate analogue was only soluble upon cooling. As expected, all sulfone-based polymer analogues were non-soluble in water or alcohols as other polar, protic solvents (*e.g.* MeOH, EtOH). This demonstrates, that sulfone groups show a less pronounced ability to form strong hydrogen bonds and highlights the unique nature of the tunable amphiphilic sulfoxide polymers. In addition, these different solution properties

of sulfoxides and sulfones support our assumption of using the sulfoxide oxidation as second trigger to change polymer solubility.

Looking into polymer solubility in more detail, temperature-dependent (5–90 °C) optical transmission measurements were performed to examine the temperature-responsiveness. As shown in Fig. 2a, a clear trend can be observed between an increasing alkyl group length and a reduced water solubility. While the sulfoxide polymers with a methyl P(Me-SEMA) or an ethyl group P(Et-SEMA) were completely water soluble over the whole investigated temperature range, the incorporation of an isopropyl P(iPr-SEMA) or *n*-propyl group P(*n*Pr-SEMA) results in the occurrence of distinct cloud point temperatures. Adding one further –CH$_3$ group (*n*-butyl) renders the *meth*acrylate polymer P(*n*Bu-SEMA) completely water insoluble in the examined temperature range. This trend can be further expanded to the acrylate polymers. As mentioned before, the tunability of the amphiphilic balance in our polymers is not only determined by the change in the alkyl groups' length but also by changing the polymeric backbone itself. Here, the polyacrylate backbone is less hydrophobic and as consequence, the isopropyl polyacrylate derivative P(iPr-SEA) is completely water-soluble. This is in stark contrast to its poly*meth*acrylate analogue P(iPr-SEMA). On the other hand, the *n*-propyl and *n*-butyl-sulfoxide polyacrylates P(*n*Pr-SEA) and P(*n*Bu-SEA) are observed to exhibit cloud point temperatures (Fig. 2a).

Interestingly, three sulfoxide polymers P(*n*Bu-SEA)$_{119}$, P(*n*Pr-SEMA)$_{130}$ and P(iPr-SEMA)$_{128}$, that show a cloud point, are constitutional isomers. However, the polymer backbone and the different alkyl groups influence the temperature range in which the cloud point occurs very drastically. This can be seen in the respective transmittance *versus* temperature curves in Fig. 2b. From these curves, the cloud point temperatures were obtained as the minimum in plots of the first derivative (inflection point) against temperature (see ESI section V, Fig. S6†).[46] From these measurements, it was determined that the polyacrylate P(*n*Bu-SEA)$_{119}$ exhibits a cloud point temperature at 11 °C, whereas the T_{cp} of the poly*meth*acrylate isomer P(*n*Pr-SEMA)$_{130}$ is at 36 °C. Thus, the shorter *n*-propyl side group but additional methyl group in the backbone shift the T_{cp} close to human body temperature. In comparison, the T_{cp} of the isopropyl isomer P(iPr-SEMA)$_{128}$ is increased significantly to 63 °C (Fig. 2b). Such a higher T_{cp} for the isopropyl polymer compared to the *n*-propyl-analogue has also been reported for poly(*N*-alkyl acrylamides). For example, the T_{cp} of poly(*N*-*n*-propyl acrylamide) (PNNPAM) (22 °C) is also decreased compared to its structural isomer poly(*N*-isopropyl acrylamide) (PNIPAM) (32 °C).[47]

In addition to T_{cp} changes between the constitutional isomers, the cloud point also changed with the polymer backbone. By comparing the poly*meth*acrylate and the polyacrylate with the same *n*-propyl group, a 35 °C increase in cloud point temperature from P(*n*Pr-SEMA)$_{130}$ with T_{cp} = 36 °C to P(*n*Pr-SEA)$_{124}$ with T_{cp} = 71 °C (Fig. 2a) is observed. This shift of T_{cp} in dependence on the backbone is in accordance to literature
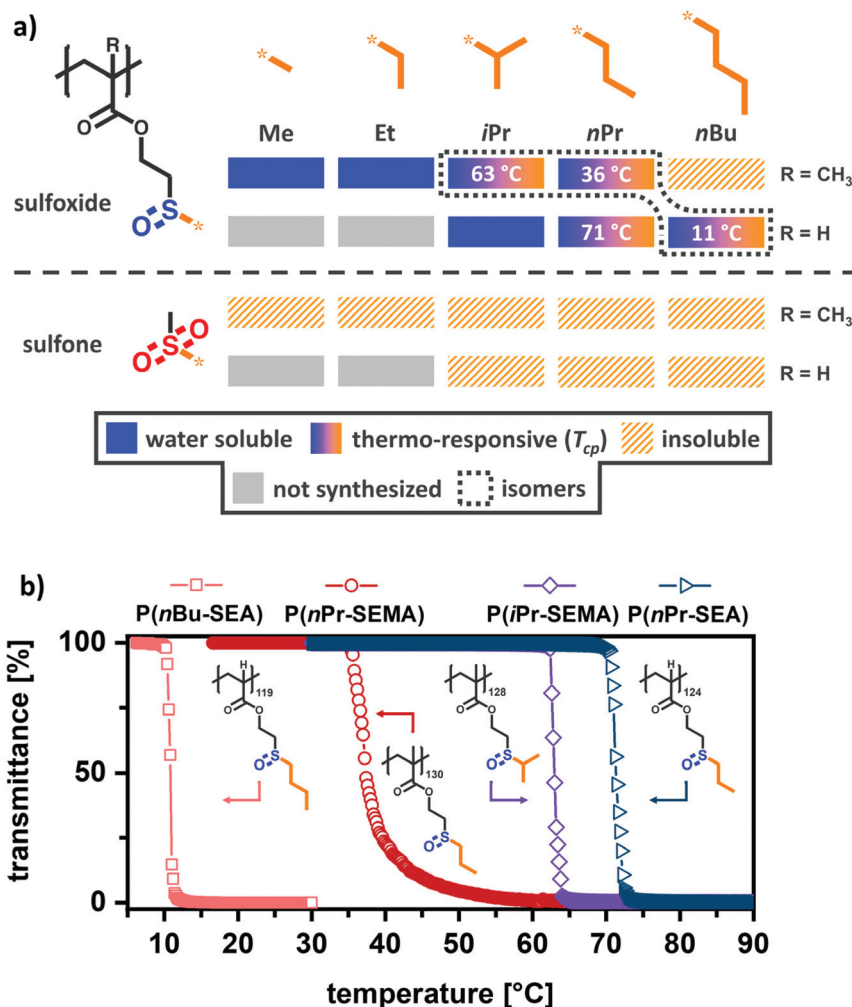
Fig. 2 Overview of the temperature-dependent solution properties of sulfoxide and sulfone-based (meth)acrylate polymers. (a) Variation of alkyl length and backbone architecture induces a shift in amphiphilicity and thermo-responsive behavior, while the oxidized hydrophobic sulfone analogues are all water insoluble. (b) Of this library, the polymers P(nBu-SEA)₁₁₉, P(nPr-SEMA)₁₃₀, P(iPr-SEMA)₁₂₈, and P(nPr-SEA)₁₂₄ were observed to exhibit distinct cloud point temperatures of 11 °C, 36 °C, 63 °C and 71 °C, respectively.

where it was described for oligo(ethylene glycol) *meth*acrylates and oligo(ethylene glycol) acrylates.[48,49]

As a consequence, the observed order of increasing cloud point temperature for the sulfoxide polymers P(nBu-SEMA) < P(nPr-SEMA) < P(iPr-SEMA) < P(nPr-SEA) agrees with established concepts.[50]

Detailed investigations on the RAFT polymerization of P(nPr-SEMA) and P(iPr-SEMA) as most promising functional polymers

Regarding potential applications, the polymers with cloud points above room temperature are of special interest. However, the utilization of such polymers in advanced materials requires a thorough understanding and control over the polymerization process itself (conversion, molecular weight, polymer dispersity, *etc.*). This would enable the synthesis of precisely tailored and complex polymer architectures such as functional block copolymers *etc.* To examine the level

of control that can be achieved with the RAFT process, polymerization kinetics are assessed in detail for the nPr-SEMA and the iPr-SEMA monomers. Fig. 3a shows the conversion of nPr-SEMA during the polymerization. It can be seen that the monomer conversion increases rapidly to 64% in the first 8 hours and then reaches a plateau at around 82% with increasing polymerization time. As seen in the kinetic plot of $\ln([M]_0/[M])$ *versus* polymerization time in Fig. 3b, a linear correlation can be observed in the initial 8 h suggesting a constant number of active species. Taking the whole reaction time into account, however, the polymerization follows pseudo-first order kinetics. In a similar fashion, the RAFT polymerization of the isomer iPr-SEMA exhibits a conversion of 67% in the initial 8 hours with a plateau at around 75% (Fig. 3e) and similar polymerization kinetics (Fig. 3f). The slight deviation of monomer conversion from the ideal case of 100% may originate from the lower reactivity of the monomers. This could lead to increased chain termination processes which are in
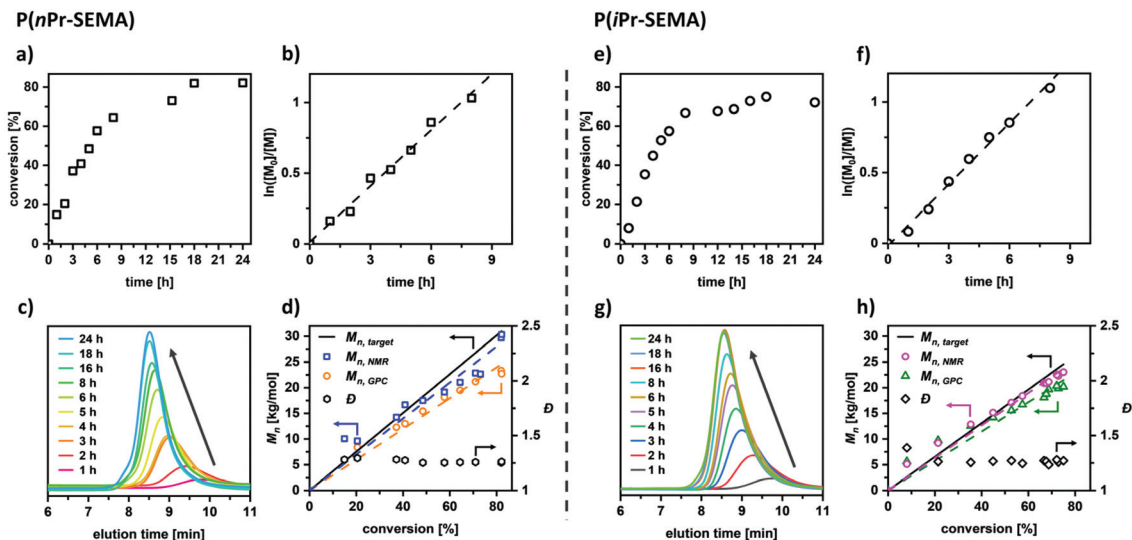
P(*n*Pr-SEMA)

P(*i*Pr-SEMA)

Fig. 3 RAFT solution homopolymerization of 2-(*n*-propyl sulfoxide)ethyl *meth*acrylate (*n*Pr-SEMA) and 2-(isopropyl sulfoxide)ethyl *meth*acrylate (iPr-SEMA) shows good control over the polymerization kinetics. (a and e) Monomer conversion and (b and f) kinetic plots of ln([M]$_0$/[M]) *versus* polymerization time, (c and g) GPC traces as a function of elution time and (d and h) number-average molecular weights (M_n) and polymer dispersity (*Đ*) *versus* overall conversion under an initial feed ratio of [monomer]$_0$: [CDTB]$_0$: [AIBN]$_0$ = 150 : 1 : 0.125.

competition with the propagation of the polymer chain at the late stage of the polymerization.[43]

The respective GPC traces for the RAFT homopolymerizations confirm that the molecular weight grows faster in the initial 8 h, as shown by the decreasing shift of the GPC peaks with longer reaction times (see Fig. 3c for *n*Pr-SEMA and Fig. 3g for iPr-SEMA). In addition to kinetic plots, the dependence of the molecular weight on the conversion serves as measure for the control over the system. For both investigated monomers (*n*Pr-SEMA and iPr-SEMA), the number-average molecular weights $M_{n,GPC}$ and $M_{n,NMR}$ increase linearly with the monomer conversion. The molecular weight distributions remain relatively narrow throughout the whole polymerization process (*Đ* ≤ 1.25). As shown in Fig. 3d for *n*Pr-SEMA and Fig. 3h for iPr-SEMA, the measured values for $M_{n,\ GPC}$ are slightly lower than the calculated targeted molecular weight $M_{n,\ target}$. This might stem from the determination of the GPC values in comparison to PMMA calibration standards. In contrast, the values for $M_{n,\ NMR}$ agree well with the theoretical molecular weights. Overall, the presented kinetic data demonstrate good control over the RAFT polymerization reaction, thus highlighting the potential of these versatile functional monomers for advanced polymeric materials.

Detailed studies on the thermo-responsive properties of P(*n*Pr-SEMA) and P(*i*Pr-SEMA)

Having demonstrated good control over the RAFT polymerization of P(*n*Pr-SEMA) and P(iPr-SEMA), their thermo-responsive properties are assessed in more detail. It is known that the cloud point temperature (T_{cp}) of thermo-responsive polymers can depend on molecular weight, polymer concentration and salt concentration. Thus, it is of great importance to assess the

influence of these parameters to gain a thorough understanding of the polymer properties.

To examine the influence of polymer molecular weight, *i.e.* degree of polymerization (DP), additional polymers of varying chain lengths were synthesized (see ESI section VI, Table S3† for details). The respective DPs were 45, 130, and 213 for P(*n*Pr-SEMA) and 48, 128, and 209 for P(iPr-SEMA). Comparing the temperature-dependent solubility of these polymers, it is observed that T_{cp} decreases with increasing polymer chain length for both polymers in solution (0.5 wt%). See Fig. 4a and d for temperature-dependent transmittance curves for P(*n*Pr-SEMA) and P(iPr-SEMA), respectively. For P(*n*Pr-SEMA), the T_{cp} decreases from 43 to 31 °C as the DP increases from 45 to 213. Thus, this polymer shows a moderate influence of the DP on the temperature response, which is similar to other typical thermo-responsive polymers like PNIPAM. Hence, the T_{cp} is robust against changes in polymer chain length. This is also the case for P(iPr-SEMA). Here, T_{cp} decreases from 71 °C to 61 °C as the DP increases from 48 to 209 (Fig. 4d). As known from other thermo-responsive polymers, this behavior is attributed to an increase in functional groups (alkyl sulfoxides) per polymer chain with increasing molecular weight. As a consequence, the net gain of free energy increases with an increased number of temperature-induced hydrophobic associations and released water molecules.[50]

Based on these findings, we assessed the influence of polymer dispersity, *i.e.* the width of the molecular weight distribution, on the T_{cp}. For this, free radical polymerizations were conducted to obtain polymers with comparable molecular weights but drastically higher dispersity values between *Đ* = 2.9 and 3.3 (see ESI section VII, Fig. S7 and S8†). For these free radical polymers, the observed effect of M_n on the T_{cp} is
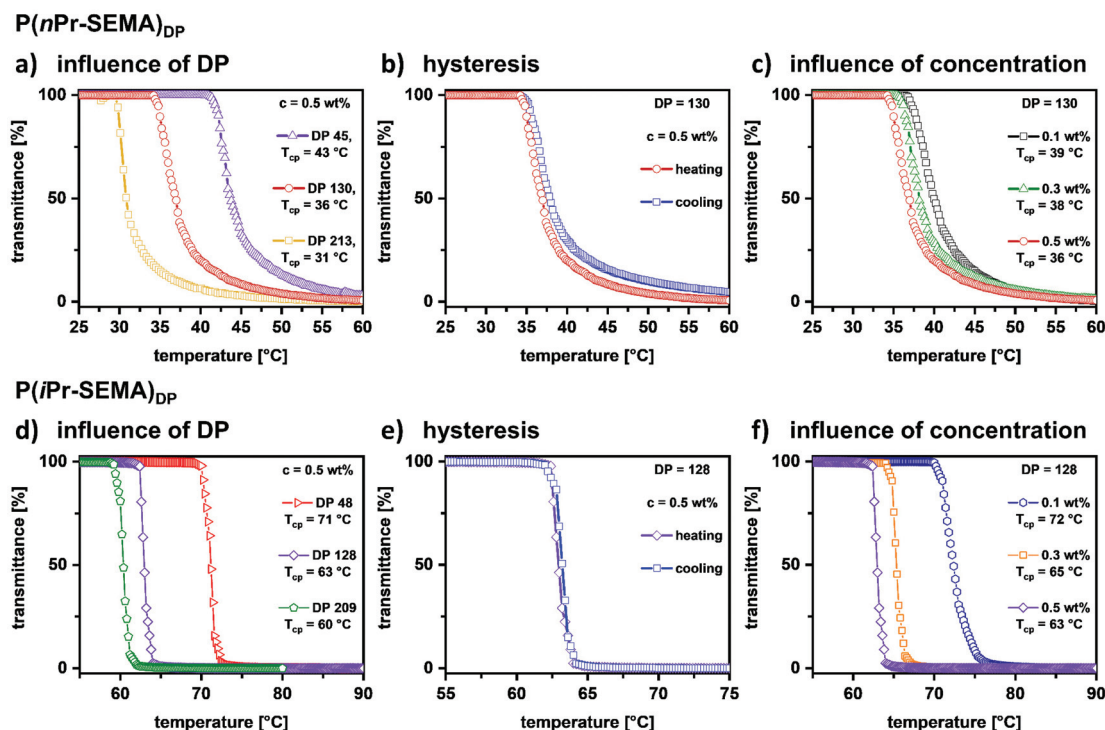
Fig. 4 Detailed temperature-responsive examinations on P(iPr-SEMA) and P(nPr-SEMA) in aqueous solution to study the effect of: (a and d) changing the polymer molecular weight; (b and e) the heating or cooling cycle (hysteresis); and (c and f) the polymer concentration.

only marginal. This indicates that for such broad molecular weight distributions, the difference between a M_n of 14 000 g mol^{-1} and 28 900 g mol^{-1} is not as significant as for the corresponding RAFT polymers with much narrower dispersities. For these RAFT polymers with dispersities of around $Đ = 1.2$ to 1.3, the difference in T_{cp} is much more evident. This indicates the importance of low dispersity values for tunability of the thermo-responsive properties by the adjustment of the molecular weight (for a detailed discussion see ESI section VII†).

Furthermore, the influence of heating and cooling on the temperature-dependent phase transition was assessed for both polymers. This serves as a measure for the reversibility and robustness of the observed cloud point temperatures. Fig. 4b and e show the heating and cooling curves for P(nPr-SEMA)$_{130}$ and P(iPr-SEMA)$_{128}$, respectively (see ESI section VIII† for additional hysteresis curves). For all polymers these curves are nearly overlapping, thus not showing a pronounced hysteresis. This can be attributed to the lack of H-bond donors in their molecular structures. In general, during the cooling process, polymers that contain both (H-acceptors and H-donors) will form polymer–water H-bonds while also replacing the additional polymer–polymer H-bonds.[35] Hence, such polymers will exhibit a thermo-responsive hysteresis.[51] However, polymers without such proton donors were found to exhibit no hysteresis since no polymer–polymer H-bonds need to be overcome.[52] As example for the latter, the new sulfoxide-based thermo-responsive polymers show distinct cloud point temp-

eratures independent from the direction of the temperature change.

Next, the concentration-dependency of the transition temperatures was investigated as shown in Fig. 4c and f. With increasing polymer concentration from 0.1 to 0.5 wt%, the T_{cp} decreases from 39 °C to 36 °C for P(nPr-SEMA)$_{130}$ and from 72 °C to 63 °C for P(iPr-SEMA)$_{128}$, respectively. Also, the transition temperature range becomes slightly broader upon dilution. This well-documented effect is based on preferential intermolecular hydrophobic aggregation of the polymers at higher concentrations. Thus, a more concentrated polymer solution results in a lower T_{cp} and a narrower transition zone. Overall, a marginal deviation of 3 °C for the P(nPr-SEMA)$_{130}$ highlights the robustness of the phase transition temperature against concentration effects, thus increasing its potential for applications.[50]

Ultimately, the influence of the salt concentration is examined since it is known that salt can reduce the transition temperature. Thus, determining this influence is important to assess the potential of the polymers for different applications where salts are present, *e.g.* in biological environments such as blood, mucus, *etc*. To analyze this behavior, sodium chloride was used as a typical example to influence the ionic strength of the polymer solutions. The temperature-dependent transmittance curves for both polymers were determined in dependence on $c(NaCl)$ (Fig. 5a for P(nPr-SEMA)$_{130}$ and Fig. 5c for P(iPr-SEMA)$_{128}$). As expected, the cloud point temperature of both polymers decreases with increasing the sodium chloride

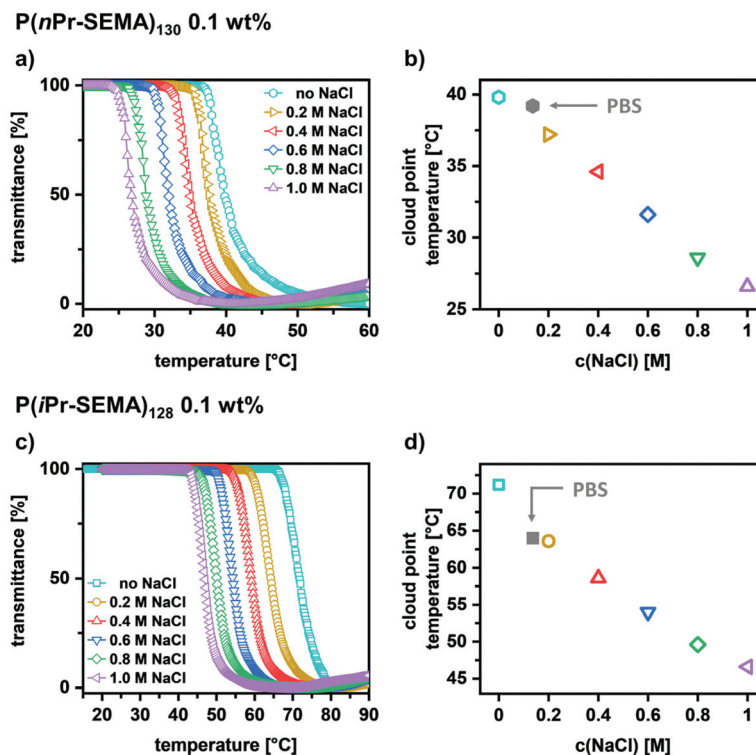**P(nPr-SEMA)₁₃₀ 0.1 wt%**

P(iPr-SEMA)₁₂₈ 0.1 wt%

Fig. 5 Influence of the sodium chloride concentration on the cloud point temperature of aqueous (a) P(nPr-SEMA)$_{130}$ and (c) P(iPr-SEMA)$_{128}$ solutions (0.1 wt%) showing the common observed "salting-out"-effect for thermo-responsive polymers. A linear dependency of the T_{cp} values on the salt concentration was observed for both polymers (b and d).

concentration from 0 to 1 M. For P(nPr-SEMA)$_{130}$ T_{cp} decreases from 40 °C to 27 °C and for P(iPr-SEMA)$_{128}$ from 71 °C to 47 °C (Fig. 5a and c). This trend becomes more evident if the T_{cp} values are plotted against the sodium chloride concentration. As shown in Fig. 5b for P(nPr-SEMA)$_{130}$ and Fig. 5d for P(iPr-SEMA)$_{128}$, both polymers exhibit a linear dependence of T_{cp} on the salt concentration. In addition, the thermal response in phosphate buffered saline (PBS) solution as a biologically more relevant environment was analyzed. Here, a T_{cp} of 39 °C for P(nPr-SEMA)$_{130}$ and 64 °C P(iPr-SEMA)$_{128}$ was observed which is in good agreement with the total sodium chloride concentration of 137 mM in PBS (Fig. 5b for P(nPr-SEMA)$_{130}$, Fig. 5d for P(iPr-SEMA)$_{128}$, see ESI section IX, Fig. S10† for respective transmittance curves). Overall, these results agree with the literature where the so-called "salting-out"-effect is often observed for thermo-responsive polymers. Salt ions disrupt the hydrogen-bonds between water molecules and polymer chains, thus promoting the hydrophobic polymer–polymer interactions. As a result, the transition temperatures decrease.

Oxidation-responsive properties of P(nPr-SEMA) and P(iPr-SEMA)

Due to the sulfoxide groups, the thermo-responsive phase transition of P(nPr-SEMA) and P(iPr-SEMA) is expected to change upon oxidation to the respective sulfone moieties. It is assumed that an increasing degree of oxidation, i.e. increasing

sulfone content, per polymer decreases the homopolymer hydrophilicity, thus shifting T_{cp} to lower temperatures.

These anticipated shifts in thermal response were investigated for P(nPr-SEMA)$_{130}$ and P(iPr-SEMA)$_{128}$. For this, the respective aqueous polymer solutions (0.1 wt%) were first subjected to different hydrogen peroxide concentrations for 6 hours at 37 °C. Hydrogen peroxide was used here as a more biological relevant oxidizing agent. ^{1}H-NMR investigations on the resulting polymers revealed partial oxidation of the sulfoxides to sulfone side groups (see ESI section X† for details). Thus, as a response to the reactive oxygen species in H$_2$O$_2$, the sulfoxide homopolymers are transformed into copolymers containing sulfoxide and sulfone side groups (Fig. 6a). Here, the content of sulfone groups increases with the H$_2$O$_2$ concentration and dramatically influences the transition temperatures. This can be seen from the temperature-dependent transmittance measurements shown in Fig. 6b for P(nPr-SEMA)$_{130}$ and Fig. 6e for P(iPr-SEMA)$_{128}$ at 0.1 wt% polymer concentration.

For P(nPr-SEMA)$_{130}$, the native non-oxidized polymer exhibits a T_{cp} at 41 °C. With increasing oxidation of hydrophilic sulfoxide groups to more hydrophobic sulfones, this T_{cp} is decreasing to 32 °C for a sulfone content of 12 mol% (Fig. 6d). Regarding the structural isomer P(iPr-SEMA)$_{128}$, the decrease of T_{cp} from 72 °C (non-oxidized) to 46 °C (sulfone content of around 13 mol%) is much more significant (Fig. 6g). For both polymers, this partial oxidation leads to random amphiphilic
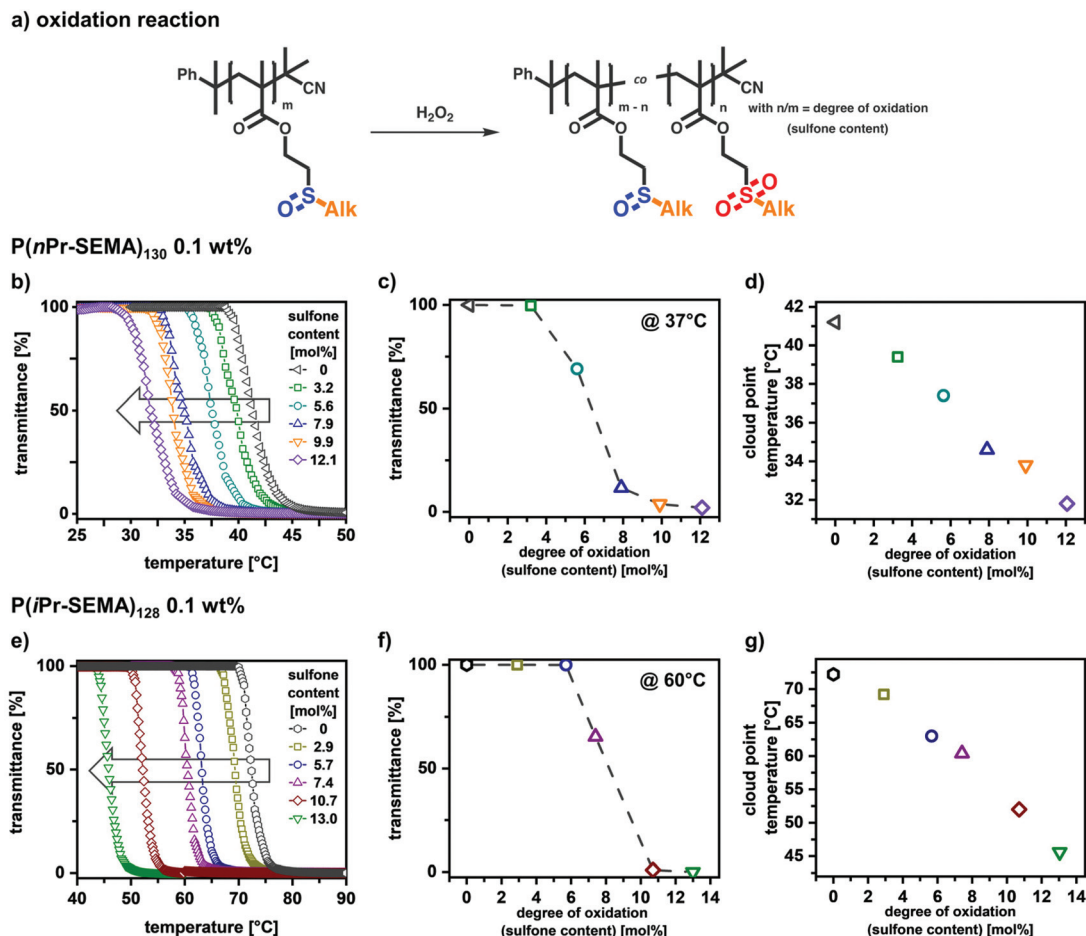
a) oxidation reaction

with n/m = degree of oxidation
(sulfone content)

P(nPr-SEMA)$_{130}$ 0.1 wt%

b)

sulfone content [mol%]
- 0
- 3.2
- 5.6
- 7.9
- 9.9
- 12.1

c) @ 37 °C

d)

P(iPr-SEMA)$_{128}$ 0.1 wt%

e)

sulfone content [mol%]
- 0
- 2.9
- 5.7
- 7.4
- 10.7
- 13.0

f) @ 60 °C

g)

Fig. 6 Demonstration of the oxidation-responsive behavior of P(nPr-SEMA)$_{130}$ and P(iPr-SEMA)$_{128}$. (a) Transformation of sulfoxide homopolymers into copolymers containing sulfoxide and sulfone side groups occurs *via* a facile oxidation reaction with H_2O_2. (b and e) The oxidation-induced shifts in cloud point temperature are presented as temperature-dependent transmittance curves for the partially oxidized P(nPr-SEMA)$_{130}$ and P(iPr-SEMA)$_{128}$ (0.1 wt% solutions). (c and f) At a fixed temperature, *e.g.* 37 °C for P(nPr-SEMA)$_{130}$ and 60 °C for P(iPr-SEMA)$_{128}$, the solubility depends drastically on the degree of oxidation. (d and g) The T_{cp} decrease linearly with the degree of oxidation, thus demonstrating the ability to gradually adjust the thermo-responsive profile *via* application of the second oxidation stimulus.

copolymers which assemble into colloidal aggregates with different sizes in aqueous dispersion above the respective T_{cp} (see ESI section XI† for further information). In contrast, for sulfone contents over 20 mol% both polymers become completely water insoluble.

These results demonstrate two important aspects; first, a clear oxidation-responsive behavior was shown for P(nPr-SEMA) and P(iPr-SEMA). At a specific constant temperature, the polymer solubility clearly depends on the oxidation state of the sulfur-based side groups and the degree of oxidation. As shown in Fig. 6c for P(nPr-SEMA), this becomes interesting for the oxidation reaction at 37 °C. Here, a dramatic decrease in solubility occurs upon reaching a sulfone content of around 6.5 mol%. Similar effects are observed for P(iPr-SEMA). However, since here the T_{cp} is shifted to higher temperatures, its oxidation-dependent solubility was shown at 60 °C. At this exemplary temperature, a dramatic decrease in transmittance was observed upon reaching a sulfone content of around

8 mol% (Fig. 6f). Consequently, this oxidation sensitivity can be used to induce "smart" materials' responses at fixed temperatures.

Second, in addition to this oxidation response, the partial oxidation of the monomeric units can also be used as synthetic concept to tune the T_{cp} of P(nPr-SEMA) and P(iPr-SEMA) very precisely. Upon oxidation, the sulfoxide-based homopolymers are transformed into copolymers containing both sulfoxide and sulfone groups randomly distributed along the same backbone. The balance between hydrophilicity (sulfoxide groups) and hydrophobicity (sulfone groups) can be varied accurately by the degree of oxidation. This results in a well-defined linear dependency between T_{cp} and the sulfone content (Fig. 6d for P(nPr-SEMA) and Fig. 6g for P(iPr-SEMA)) and allows for the precise tuning of the thermo-responsive polymer properties. A similar control is mostly realized *via* copolymer systems. However, copolymerization of two monomers always requires the synthesis of a new batch to vary the
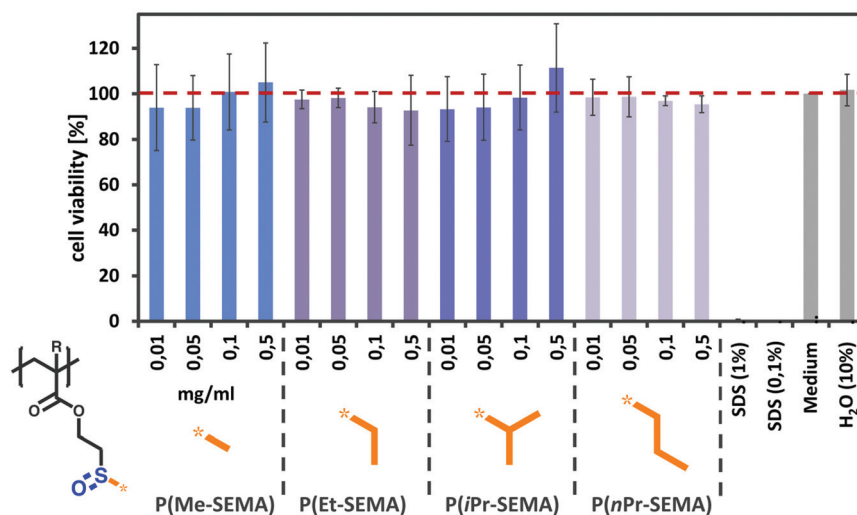
Fig. 7 Cell viability tests on cultured subcutaneous connective tissue cells (L929) show no pronounced cytotoxic effects, thus suggesting good biocompatibility of the functional polymers. Cell viability is presented as percentage with respect to the medium and as mean $\pm$ SD ($n = 3$). The data were assessed *via* the CCK-8 assay after exposure of the cells to aqueous solutions of the respective sulfoxide *metha*crylates (0.01, 0.05, 0.1, and 0.5 mg mL^{-1}) for 24 hours.

composition. Since this can also result in varying molecular weights and polymer dispersities, our oxidative post-polymerization modification approach drastically simplifies this tunability.

Demonstrating good biocompatibility *via* basic toxicological tests

Having demonstrated tunable thermo-responsive properties of the sulfoxide polymers, their biocompatibility was assessed *via in vitro* cell viability experiments. Since P(nPr-SEMA) exhibits a T_{cp} near body temperature, it is important to exclude potential polymer cytotoxicity in order to demonstrate the potential of our materials for applications in the biomedical field.

For this, the cell counting kit-8 (CCK-8) colorimetric assay was conducted on cultured subcutaneous connective tissue cells of mice (L929). This cell type is used among others as standard biological material to assess the tolerability of polymeric materials in an *in vitro* environment.[53–55] The tests were performed with four different polymer concentrations of 0.01, 0.05, 0.1, and 0.5 mg mL^{-1} and incubated for 24 hours at 37 °C. Non-cell treated medium was used as control.

The results of the CCK-8 assay are shown in Fig. 7 and indicate that all tested functional sulfoxide polymers are well tolerated by L929 cells after 24 hours. Overall, this supports good biocompatibility of the presented dual-functional sulfoxide polymers. These biological properties were already shown for methyl sulfoxide acrylates which is regarded as potential PEG alternative.[36,41] However, it is of great importance to show this non-toxic behavior also for our sulfoxide polymers with increasing hydrophobic alkyl groups. While such amphiphilic structures may present undesired hydrophobic interactions with the cell membrane, no significant influence on the cell viability was observed. This highlights the potential of our

multi-stimuli-responsive sulfoxide homopolymers to be utilized for a variety of biological applications.

Conclusion

We have demonstrated that a rational molecular design can be used to introduce thermo- and oxidation-responsive properties into one functional monomer. Key to this approach is the combination of highly hydrophilic sulfoxide moieties with varying hydrophobic alkyl groups.

By systematically investigating the influence of different structural parameters, *i.e.* alkyl groups, polymer backbone, degree of polymerization (DP), this study lays the foundation for the preparation of new materials with well-defined and robust thermo-responsive profiles. As one promising candidate, P(nPr-SEMA) was found to exhibit a cloud point temperature close to human body temperature, thus making the thermal-response attractive for potential biomedical applications. Regarding the dual-stimuli-responsive properties, combining the thermal-response with an oxidation-sensitivity represents a unique way to realize more complex response profiles.

On one hand, this is achieved through the oxidation-dependent shift of the polymer's solubility at a fixed temperature. On the other hand, this allows to precisely tune the cloud point temperature by altering the balance between hydrophilic sulfoxide groups and hydrophobic sulfone groups. In contrast to this simple post-polymerization oxidation strategy, a similar control was mostly realized *via* copolymer systems. However, copolymerization of two monomers always requires the synthesis of a new batch to vary the composition which can influence molecular weights and polymer dispersities. By simplifying this tunability of thermo-responsiveness, our approach rep-

resents a simple yet powerful expansion of the functional polymer toolbox.

Overall, we believe that combining the thermal and oxidation response in one single functional unit, its facile synthesis, and well-controlled polymerization, presents the starting point for the preparation of highly sophisticated materials for a wide variety of applications.

Materials and methods

Materials

All starting materials and reagents were purchased from commercial sources and used without further purification, unless otherwise stated. Methacryloyl chloride (97%) and triethylamine (99%) were purchased from abcr GmbH. Anhydrous *N*,*N*-dimethylformamide (DMF, 99.8%, extra dry, stored over molecular sieve) was purchased from Acros Organics. 2-(Methylthio)ethan-1-ol, 2-(ethylthio)ethan-1-ol, 2-(i-propylthio)ethan-1-ol, 2-(n-propylthio)ethan-1-ol, 2-(n-butylthio)ethan-1-ol and *p*-toluenesulfonic acid monohydrate were purchased from Fluorochem Ltd. Acryloyl chloride (stabilized with phenothiazine) and α-methylstyrene (99%) were purchased from Merck KGaA. 2,2′-Azobis(2-methylpropionitrile) (AIBN, 98%), carbon disulfide (≥99.9%), 2,6-di-*tert*-butyl-*p*-cresol (>99%), *meta*-chloroperbenzoic acid (*m*CPBA, ≥77%) and phenyl magnesium bromide solution (1 M in THF) were purchased from Sigma-Aldrich. Cumyl dithiobenzoate (CDTB) was synthesized according to literature procedures.[56] Ultrapure water was taken from a LaboStar UV 2 water system. Moisture and/or air sensitive reactions were carried out in dry glassware under nitrogen atmosphere.

Nuclear magnetic resonance spectroscopy. ^{1}H and ^{13}C NMR spectra were recorded at 300 K on a JEOL ECP 500 spectrometer operating at 500 MHz and on a JEOL ECZ600 spectrometer operating at 600 MHz. The chemical shifts (δ) are expressed in parts per million (ppm) while coupling constants (J) are stated in hertz (Hz). Coupling patterns are differentiated into s (singlet), d (doublet), t (triplet), q (quartet) including their combinations and as m (multiplet).

Gel permeation chromatography (GPC). The number-average molecular weights (M_n) and molecular weight distributions (M_w/M_n) of polymers were determined using a customized GPC system operating with DMF at 50 °C and comprising two PSS SDV linear M 5 µm particle size columns (5 cm and 30 cm) connected in series to a PSS SECcurity RI differential refractometer detector. HPLC-grade DMF with 10 mmol lithium bromide was used as eluent at a flow rate of 1.0 mL min^{-1}. Calibration was conducted using poly(methyl *meth*acrylate) standards (M_n = 600–1 600 000 g mol^{-1}). Polymer sample solutions (1.5 mg ml^{-1}) were prepared in the GPC eluent and filtered (PTFE, 450 µm) prior to injection. Chromatograms were processed using the PSS WinGPC UniChrom software.

Temperature-dependent transmittance studies: turbidimetry. Turbidity measurements were performed on a Lambda 950 UV/Vis/NIR spectrophotometer at a fixed wavelength of

λ = 500 nm with a PTP-6 Peltier Temperature Programmer (PerkinElmer Life and Analytical Sciences, Massachusetts, USA). Cloud point temperatures (T_{cp}'s) of polymer solutions were measured in ultrapure water at concentrations of 0.1–0.5 wt% by applying a heating rate of 0.5 °C min^{-1} with data point recordings every 0.2 °C. The T_{cp} represents the temperature at the inflection point of the normalized transmittance *versus* temperature curve.

Cell viability studies. All cell experiments were conducted according to German genetic engineering laws and German biosafety guidelines in the laboratory (safety level 1). Cell viability was determined using a CCK-8 kit (Sigma-Aldrich) according to the manufactor's instructions. L929 cells were obtained from Leibniz-Institut DSMZ – Deutsche Sammlung von Mikroorganismen und Zellkulturen GmbH and cultured in RPMI 1640 medium supplemented with 10% (v/v) FBS, 100 U mL^{-1} penicillin and 100 µg mL^{-1} streptomycin. L929 cells were seeded in a 96-well plate at a density of 5×10^4 cells per mL in 90 µl RPMI medium per well over night at 37 °C and 5% CO$_2$. 10 µl of sample (solved in deionized water) were added in serial dilutions including positive (1% SDS) and negative controls (medium, H$_2$O) and incubated for another 24 h at 37 °C and 5% CO$_2$. For background subtraction, also wells containing no cells but only sample were used. After 24 h incubation the CCK8 solution was added (10 µl per well) and absorbance (450 nm/650 nm) was measured after approximately 3 h incubation of the dye using a Tecan plate reader (Infinite pro200, TECAN-reader Tecan Group Ltd). Measurements were performed in triplicates and repeated three times. The cell viability was calculated by setting the non-treated control to 100% and the non-cell control to 0% after subtracting the background signal using the Excel software.

Syntheses

Syntheses of 2-(*alkyl*-thio)ethyl (meth)acrylates (*alkyl*-TE(M)A). In a typical reaction, methacryloyl chloride (9.20 g, 88.0 mmol) or acryloyl chloride (8.10 g, 88.0 mmol), respectively, were added dropwise to a solution of the respective 2-(*alkyl*-thio) ethan-1-ol (80.0 mmol) in 90 mL DCM at 0 °C. Subsequently, triethylamine (8.91 g, 88.0 mmol) was added dropwise to the reaction mixture which was then allowed to reach room temperature while stirring overnight. The precipitate was then filtered off and the filtrate was washed three times with saturated sodium bicarbonate and once with brine before drying over sodium sulfate. A spatula tip of di-*tert*-butyl-*p*-cresol was added to the solution as polymerization inhibitor. After the solvent was removed the crude product was either distilled under reduced pressure or purified *via* column chromatography to give pale yellowish liquids.

Me-TEMA (chromatography: DCM/methanol 3 v/v%; yield 92%) ^{1}H NMR (500 MHz, CDCl$_3$): δ = 6.12 (s, 1H, H$_{cis}$), 5.57 (s, 1H, H$_{trans}$), 4.32 (t, J = 6.9 Hz, 2H, –O–CH$_2$–), 2.76 (t, J = 6.9 Hz, 2H, –CH$_2$–O–), 2.16 (s, 3H, –S–CH$_3$), 1.94 (s, 3H, –CH$_3$) ppm; ^{13}C NMR (126 MHz, CDCl$_3$): δ = 167.33, 136.28, 125.91, 63.55, 32.71, 18.42, 15.98 ppm; HRMS: calc. for C$_7$H$_{12}$O$_2$S [M + H]$^+$: 161.0636, found [M + H]$^+$: 161.0641.

Et-TEMA (chromatography: DCM/methanol 3 v/v%; yield 88%) ^{1}H NMR (500 MHz, CDCl$_3$): δ = 6.11 (s, 1H, H$_{cis}$), 5.57 (s, 1H, H$_{trans}$), 4.29 (t, J = 7.0 Hz, 2H, –O–CH$_2$–), 2.79 (t, J = 7.0 Hz, 2H, –CH$_2$–S–), 2.60 (q, J = 7.5 Hz, 2H, –S–CH$_2$–), 1.94 (s, 3H, –CH$_3$), 1.26 (t, J = 7.4 Hz, 3H, –CH$_2$–$\underline{CH}_3$) ppm; ^{13}C NMR (126 MHz, CDCl$_3$): δ = 167.32, 136.30, 125.89, 64.06, 30.10, 26.34, 18.42, 14.94 ppm; HRMS: calc. for C$_8$H$_{14}$O$_2$S [M + K]$^+$: 213.0352, found [M + K]$^+$: 213.0554.

iPr-TEMA (distillation: 0.12 mbar, 39–42 °C; yield 71%) ^{1}H NMR (500 MHz, CDCl$_3$): δ = 6.12 (s, 1H, H$_{cis}$), 5.58 (t, J = 1.6 Hz, 1H, H$_{trans}$), 4.28 (t, J = 7.1 Hz, 2H, –O–CH$_2$–), 3.00 (p, J = 6.7 Hz, 1H, –S–CH–), 2.80 (t, J = 7.1 Hz, 2H, –CH$_2$–S–), 1.94 (s, 3H, –CH$_3$), 1.28 (d, J = 6.7 Hz, 6H, (–CH$_3$)$_2$) ppm; ^{13}C NMR (126 MHz, CDCl$_3$): δ = 167.34, 136.32, 125.90, 64.34, 35.23, 29.00, 23.57, 18.44 ppm; HRMS: calc. for C$_9$H$_{16}$O$_2$S [M + Na]$^+$: 211.0769, found [M + Na]$^+$: 211.0768.

nPr-TEMA (distillation: 0.12 mbar, 40–45 °C; yield 82%) ^{1}H NMR (500 MHz, CDCl$_3$): δ = 6.11 (s, 1H, H$_{cis}$), 5.57 (s, 1H, H$_{trans}$), 4.29 (t, J = 7.0 Hz, 2H, –O–CH$_2$–), 2.77 (t, J = 7.0 Hz, 2H, –CH$_2$–S–), 2.55 (t, 2H, –S–CH$_2$–), 1.94 (s, 3H, –CH$_3$), 1.67–1.57 (m, 2H, –$\underline{CH}_2$–CH$_3$), 0.98 (t, J = 7.3 Hz, 3H, –CH$_2$–$\underline{CH}_3$) ppm; ^{13}C NMR (126 MHz, CDCl$_3$): δ = 167.33, 136.31, 125.89, 64.09, 34.56, 30.48, 23.14, 18.43, 13.52 ppm; HRMS: calc. for C$_9$H$_{16}$O$_2$S [M + Na]$^+$: 211.0769, found [M + Na]$^+$: 211.0754.

nBu-TEMA (chromatography: DCM/methanol 3 v/v%; yield 58%) ^{1}H NMR (500 MHz, CDCl$_3$): δ = 6.11 (s, 1H, H$_{cis}$), 5.57 (s, 1H, H$_{trans}$), 4.29 (t, J = 7.0 Hz, 2H, –O–CH$_2$–), 2.78 (t, J = 7.0 Hz, 2H, –CH$_2$–S–), 2.60–2.54 (m, 2H, –S–CH$_2$–), 1.94 (s, 3H, –CH$_3$), 1.58 (dt, J = 15.0, 6.8 Hz, 2H, –S–CH$_2$–$\underline{CH}_2$–), 1.40 (dq, J = 14.6, 7.4 Hz, 2H, –$\underline{CH}_2$–CH$_3$), 0.91 (t, J = 7.4 Hz, 3H, –CH$_2$–$\underline{CH}_3$) ppm. ^{13}C NMR (126 MHz, CDCl$_3$): δ = 167.33, 136.31, 125.88, 64.10, 32.24, 31.92, 30.57, 22.06, 18.43, 13.78 ppm. HRMS: calc. for C$_{10}$H$_{18}$O$_2$S [M + Na]$^+$: 225.0925, found [M + Na]$^+$: 225.0913.

iPr-TEA (chromatography: DCM/methanol 3 v/v%; yield 48%) ^{1}H NMR (500 MHz, CDCl$_3$): δ = 6.42 (dd, J = 17.3, 1.5 Hz, 1H, H$_{cis}$), 6.12 (dd, J = 17.3, 10.5 Hz, 1H, –CH–), 5.84 (dd, J = 10.4, 1.5 Hz, 1H, H$_{trans}$), 4.30 (t, J = 7.1 Hz, 2H, –O–CH$_2$–), 2.99 (p, J = 6.7 Hz, 1H, –S–CH–), 2.80 (t, J = 7.1 Hz, 2H, –CH$_2$–S–), 1.28 (d, J = 6.7 Hz, 6H, (–CH$_3$)$_2$) ppm. ^{13}C NMR (126 MHz, CDCl$_3$): δ = 166.10, 131.21, 128.39, 64.11, 35.26, 28.99, 23.55 ppm. HRMS: calc. for C$_8$H$_{14}$O$_2$S [M + Na]$^+$: 197.0612, found [M + Na]$^+$: 197.0602.

nPr-TEA (chromatography: DCM/methanol 3 v/v%; yield 53%) ^{1}H NMR (500 MHz, CDCl$_3$): δ = 6.42 (dd, J = 17.3, 1.4 Hz, 1H, H$_{cis}$), 6.12 (dd, J = 17.3, 10.5 Hz, 1H, –CH–), 5.84 (dd, J = 10.5, 1.4 Hz, 1H, H$_{trans}$), 4.30 (t, J = 7.0 Hz, 2H, –O–CH$_2$–), 2.77 (t, J = 7.0 Hz, 2H, –CH$_2$–S–), 2.55 (t, J = 7.3 Hz, 2H, –S–CH$_2$–), 1.68–1.54 (m, 2H, –$\underline{CH}_2$–CH$_3$), 0.99 (t, J = 7.3 Hz, 3H, –CH$_3$) ppm. ^{13}C NMR (126 MHz, CDCl$_3$): δ = 166.09, 131.20, 128.38, 63.88, 34.58, 30.49, 23.13, 13.53 ppm. HRMS: calc. for C$_8$H$_{14}$O$_2$S [M + Na]$^+$: 197.0612, found [M + Na]$^+$: 197.0582.

nBu-TEA (chromatography: DCM/methanol 3 v/v%; yield 62%) ^{1}H NMR (500 MHz, CDCl$_3$): δ = 6.42 (dd, J = 17.3, 1.4 Hz, 1H, H$_{cis}$), 6.13 (dd, J = 17.3, 10.4 Hz, 1H, –CH–), 5.84 (dd, J = 10.5, 1.4 Hz, 1H, H$_{trans}$), 4.30 (t, J = 7.0 Hz, 2H, –O–CH$_2$–), 2.78

(s$_{br}$, 2H, –CH$_2$–S–), 2.58 (s$_{br}$, 2H, –S–CH$_2$–), 1.58 (p, J = 7.4 Hz, 2H, –S–CH$_2$–$\underline{CH}_2$–), 1.41 (h, J = 7.4 Hz, 2H, –$\underline{CH}_2$–CH$_3$), 0.91 (t, J = 7.4 Hz, 3H, –CH$_3$) ppm. ^{13}C NMR (126 MHz, CDCl$_3$): δ = 166.10, 131.21, 128.39, 63.90, 32.23, 31.92, 30.53, 22.06, 13.79 ppm. HRMS: calc. for C$_9$H$_{16}$O$_2$S [M + Na]$^+$: 211.0769, found [M + Na]$^+$: 211.0759.

Syntheses of 2-(alkyl-sulfoxide)ethyl (meth)acrylates (*alkyl*-SE(M)A). In a typical reaction, a solution of *m*CPBA (2.47 g, 14.3 mmol) in 30 mL DCM was added dropwise to a solution of *alkyl*-TEMA (14.3 mmol) or *alkyl*-TEA (14.3 mmol), respectively, in 30 mL DCM at 0 °C. Subsequently, the reaction mixture was allowed to reach RT while stirring overnight. The precipitate was then filtered off and the filtrate was washed three times with saturated sodium bicarbonate and once with brine before drying over sodium sulfate. A spatula tip of di-*tert*-butyl-*p*-cresol was added to the solution as polymerization inhibitor. After the solvent was removed the crude oily product was purified by column chromatography (DCM/methanol 3 v/v%) to yield colorless clear liquids or solids.

Me-SEMA (solid; yield 78%) ^{1}H NMR (500 MHz, CDCl$_3$): δ = 6.12 (s, 1H, H$_{cis}$), 5.58 (s, 1H, H$_{trans}$), 4.32 (t, J = 6.8 Hz, 2H, –O–CH$_2$–), 2.80 (s$_{br}$, 2H, –CH$_2$–SO–), 2.20 (s$_{br}$, 3H, –SO–CH$_3$), 1.94 (s, 3H, –CH$_3$) ppm. ^{13}C NMR (126 MHz, CDCl$_3$): δ = 167.32, 136.28, 129.10, 125.91, 32.63, 18.42, 18.05 ppm. HRMS: calc. for C$_7$H$_{13}$O$_3$S [M + Na]$^+$: 199.0405, found [M + Na]$^+$: 199.0414.

Et-SEMA (liquid; yield 82%) ^{1}H NMR (400 MHz, CDCl$_3$): δ = 6.14 (s, 1H, H$_{cis}$), 5.61 (s, 1H, H$_{trans}$), 4.69–4.48 (m, 2H, –O–CH$_2$–), 3.10–2.92 (m, 2H, –CH$_2$–SO–), 2.79 (qd, J = 7.5, 3.1 Hz, 2H, –SO–CH$_2$–), 1.94 (s, 3H, –CH$_3$), 1.36 (t, J = 7.5 Hz, 3H, –CH$_2$–$\underline{CH}_3$) ppm. ^{13}C NMR (101 MHz, CDCl$_3$): δ = 167.06, 135.82, 126.62, 57.60, 50.79, 46.24, 18.35, 6.89 ppm. HRMS: calc. for C$_8$H$_{14}$O$_3$S [M + Na]$^+$: 213.0561, found [M + Na]$^+$: 213.0576.

iPr-SEMA (liquid; yield 75%) ^{1}H NMR (500 MHz, CDCl$_3$): δ = 6.14 (s, 1H, H$_{cis}$), 5.61 (s, 1H, H$_{trans}$), 4.69–4.51 (m, 2H, –O–CH$_2$–), 3.06–2.94 (m, 1H, –SO–CH–), 2.92–2.81 (m, 2H, –CH$_2$–SO–), 1.94 (s, 3H, –CH$_3$), 1.31 (dd, J = 25.0, 6.9 Hz, 6H, (–CH$_3$)$_2$) ppm. ^{13}C NMR (126 MHz, CDCl$_3$): δ = 167.10, 135.88, 126.55, 57.90, 50.87, 48.06, 18.35, 16.01, 14.82 ppm. HRMS: calc. for C$_9$H$_{16}$O$_3$S [M + Na]$^+$: 227.0718, found [M + Na]$^+$: 227.0712.

nPr-SEMA (liquid; yield 85%) ^{1}H NMR (600 MHz, CDCl$_3$): δ = 6.13 (s, 1H, H$_{cis}$), 5.61 (s, 1H, H$_{trans}$), 4.69–4.48 (m, 2H, –O–CH$_2$–), 3.09–2.92 (m, 2H, –CH$_2$–SO–), 2.82–2.64 (m, 2H, –SO–CH$_2$–), 1.94 (s, 3H, –CH$_3$), 1.88–1.79 (m, 2H, –$\underline{CH}_2$–CH$_3$), 1.09 (t, J = 7.4 Hz, 3H, –CH$_2$–$\underline{CH}_3$) ppm. ^{13}C NMR (151 MHz, CDCl$_3$): δ = 167.05, 135.84, 126.60, 126.59, 57.57, 55.08, 51.62, 51.60, 18.36, 16.44, 13.50 ppm. HRMS: calc. for C$_9$H$_{16}$O$_3$S [M + Na]$^+$: 227.0718, found [M + Na]$^+$: 227.0730.

nBu-SEMA (liquid; yield 69%) ^{1}H NMR (600 MHz, CDCl$_3$): δ = 6.13 (s, 1H, H$_{cis}$), 5.60 (s, 1H, H$_{trans}$), 4.67–4.50 (m, 2H, –O–CH$_2$–), 3.11–2.93 (m, 2H, –CH$_2$–SO–), 2.85–2.68 (m, 2H, –SO–CH$_2$–), 1.94 (s, 3H, –CH$_3$), 1.82–1.71 (m, 2H, –SO–CH$_2$–$\underline{CH}_2$–), 1.58–1.40 (m, 2H, –$\underline{CH}_2$–CH$_3$), 0.96 (t, J = 7.3 Hz, 3H, –CH$_2$–$\underline{CH}_3$) ppm. ^{13}C NMR (151 MHz, CDCl$_3$): δ = 167.03, 135.82, 126.59, 57.58, 52.74, 51.46, 24.71, 22.15, 18.35, 13.78,

13.78 ppm. HRMS: calc. for $C_{10}H_{18}O_3S$ [M + Na]$^+$: 241.0874, found [M + Na]$^+$: 241.0862.

nPr-SEA (liquid; yield 85%) ^{1}H NMR (500 MHz, CDCl$_3$): δ = 6.44 (dd, J = 17.3, 1.3 Hz, 1H, H$_{cis}$), 6.13 (dd, J = 17.4, 10.5 Hz, 1H, –CH–), 5.88 (dd, J = 10.5, 1.3 Hz, 1H, H$_{trans}$), 4.68–4.51 (m, 2H, –O–CH$_2$–), 3.08–2.91 (m, 2H, –CH$_2$–SO–), 2.83–2.62 (m, 2H, –SO–CH$_2$–), 1.88–1.77 (m, 2H, –$\underline{CH_2}$–CH$_3$), 1.09 (t, J = 7.4 Hz, 3H, –CH$_3$) ppm. ^{13}C NMR (126 MHz, CDCl$_3$): δ = 131.92, 127.86, 120.04, 57.46, 54.99, 51.46, 16.42, 13.49 ppm. HRMS: calc. for $C_8H_{14}O_3S$ [M + Na]$^+$: 213.0561, found [M + Na]$^+$: 213.0563.

iPr-SEA (liquid; yield 73%) ^{1}H NMR (500 MHz, CDCl$_3$): δ = 6.44 (dd, J = 17.3, 1.3 Hz, 1H, H$_{cis}$), 6.13 (dd, J = 17.3, 10.5 Hz, 1H, –CH–), 5.87 (dd, J = 10.5, 1.3 Hz, 1H, H$_{trans}$), 4.69–4.52 (m, 2H, –O–CH$_2$–), 3.04–2.95 (m, 1H, –SO–CH–), 2.91–2.82 (m, 2H, –CH$_2$–SO–), 1.31 (dd, J = 24.6, 6.9 Hz, 6H, (–CH$_3$)$_2$) ppm. ^{13}C NMR (126 MHz, CDCl$_3$): δ = 165.85, 131.85, 127.91, 57.78, 50.93, 47.96, 15.98, 14.82 ppm. HRMS: calc. for $C_8H_{14}O_3S$ [M + Na]$^+$: 213.0561, found [M + Na]$^+$: 213.0571.

nBu-SEA (liquid; yield 77%) ^{1}H NMR (600 MHz, CDCl$_3$): δ = 6.43 (dd, J = 17.4, 1.2 Hz, 1H, H$_{cis}$), 6.12 (dd, J = 17.3, 10.5 Hz, 1H, –CH–), 5.87 (dd, J = 10.4, 1.2 Hz, 1H, H$_{trans}$), 4.70–4.49 (m, 2H, –O–CH$_2$–), 3.12–2.91 (m, 2H, –CH$_2$–SO–), 2.85–2.66 (m, 2H, –SO–CH$_2$–), 1.83–1.69 (m, –SO–CH$_2$–$\underline{CH_2}$–), 1.58–1.40 (m, 2H, –$\underline{CH_2}$–CH$_3$), 0.96 (t, J = 7.3 Hz, 3H, –CH$_3$) ppm. ^{13}C NMR (151 MHz, CDCl$_3$): δ = 165.79, 131.92, 127.83, 57.46, 52.77, 51.39, 24.68, 22.13, 13.78 ppm. HRMS: calc. for $C_9H_{16}O_3S$ [M + Na]$^+$: 227.0718, found [M + Na]$^+$: 227.0702.

RAFT homopolymerization of sulfoxide monomers. In a representative polymerization reaction, a stock solution of nPr-SEMA (360.3 mg, 1.762 mmol), CDTB (3.150 mg, 11.56 µmol) and AIBN (0.270 mg, 1.644 µmol) in 1.824 g anhydrous DMF was prepared. Aliquots (165 µL) were transferred to 1.5 mL vials. The reaction mixtures were purged with nitrogen for 20 minutes, sealed and immersed into a preheated oil bath at 75 °C with stirring. After predetermined intervals, the sealed vials were ventilated and cooled with liquid nitrogen to stop the polymerization reaction. Subsequently, samples were withdrawn for ^{1}H NMR analysis and GPC measurements. The crude polymer was then purified by precipitating twice in diethyl ether and drying *in vacuo* followed by redissolution in deionized water and lyophilization to yield the final RAFT homopolymer as a pale pink solid.

Removal auf CDTB end group. In a typical reaction, P(nPr-SEMA) (38.3 mg, 0.187 mmol) and AIBN (3.22 mg, 10.6 µmol) were dissolved in 383 µL DMF. The reaction mixture was purged with nitrogen for 20 minutes, sealed and heated to 70 °C for 4 hours while stirring. Subsequently, the crude product was purified by precipitating twice in diethyl ether and drying *in vacuo* followed by redissolution in deionized water and lyophilization to yield the final homopolymer as a colorless solid.

Synthesis of sulfone homopolymers. A solution of mCPBA (666 mg, 3.86 mmol) in 200 µL chloroform was added to a solution of P(alkyl-TEMA) (1.93 mmol) or P(alkyl-TEA), respectively, in 3 mL chloroform at 0 °C. Subsequently, the reaction mixture was allowed to reach room temperature while stirring

overnight. The crude polymer was purified by precipitating once in diethyl ether and dialysis against deionized water/methanol (5 : 1 v/v%). After a lyophilization step, the final sulfone homopolymers were yielded as colorless, fluffy solids.

Conflicts of interest

There are no conflicts to declare.

Acknowledgements

References

1 J. J. Green and J. H. Elisseeff, *Nature*, 2016, **540**, 386–394.
2 J.-F. Lutz, J.-M. Lehn, E. W. Meijer and K. Matyjaszewski, *Nat. Rev. Mater.*, 2016, **1**, 16024.
3 K. Matyjaszewski, *Prog. Polym. Sci.*, 2005, **30**, 858–875.
4 P. Schattling, F. D. Jochum and P. Theato, *Polym. Chem.*, 2014, **5**, 25–36.
5 C. M. Wells, M. Harris, L. Choi, V. P. Murali, F. D. Guerra and J. A. Jennings, *J. Funct. Biomater.*, 2019, **10**, 34.
6 L. Hu, Y. Wan, Q. Zhang and M. J. Serpe, *Adv. Funct. Mater.*, 2020, **30**, 1903471.
7 J. Qu, Q.-y. Wang, K.-l. Chen, J.-b. Luo, Q.-h. Zhou and J. Lin, *Colloids Surf., B*, 2018, **170**, 373–381.
8 M. Tang, Q. Zheng, N. Tirelli, P. Hu, Q. Tang, J. Gu and Y. He, *React. Funct. Polym.*, 2017, **110**, 55–61.
9 P. Schattling, F. D. Jochum and P. Theato, *Chem. Commun.*, 2011, **47**, 8859–8861.
10 Z. Cheng, S. Liu, P. W. Beines, N. Ding, P. Jakubowicz and W. Knoll, *Chem. Mater.*, 2008, **20**, 7215–7219.
11 S. E. Herrera, M. L. Agazzi, M. L. Cortez, W. A. Marmisollé, M. Tagliazucchi and O. Azzaroni, *Chem. Commun.*, 2019, **55**, 14653–14656.
12 S. Wang, Z. Xu, T. Wang, T. Xiao, X.-Y. Hu, Y.-Z. Shen and L. Wang, *Nat. Commun.*, 2018, **9**, 1737.
13 K. Zhang, M. Zhang, X. Feng, M. A. Hempenius and G. J. Vancso, *Adv. Funct. Mater.*, 2017, **27**, 1702784.
14 H. Zhang, W. Wu, X. Zhao and Y. Zhao, *Macromolecules*, 2017, **50**, 3411–3423.
15 T. Uemukai, T. Hioki and M. Ishifune, *Int. J. Polym. Sci.*, 2013, **2013**, 196145.
16 C. Xiao, J. Ding, L. Ma, C. Yang, X. Zhuang and X. Chen, *Polym. Chem.*, 2015, **6**, 738–747.
17 H. Fu, D. M. Policarpio, J. D. Batteas and D. E. Bergbreiter, *Polym. Chem.*, 2010, **1**, 631–633.
18 N. Kuramoto, Y. Shishido and K. Nagai, *Macromol. Rapid Commun.*, 1994, **15**, 441–444.

19 N. Kuramoto, Y. Shishido and K. Nagai, *J. Polym. Sci., Part A: Polym. Chem.*, 1997, **35**, 1967–1972.

20 N. Kuramoto and Y. Shishido, *Polymer*, 1998, **39**, 669–673.

21 C. Tonhauser, A. Alkan, M. Schömer, C. Dingels, S. Ritz, V. Mailänder, H. Frey and F. R. Wurm, *Macromolecules*, 2013, **46**, 647–655.

22 S. Matsumoto, A. Kanazawa, S. Kanaoka and S. Aoshima, *Polym. Chem.*, 2019, **10**, 4134–4141.

23 J. Huang, H. Qin, B. Wang, Q. Tan and J. Lu, *Polym. Chem.*, 2019, **10**, 6379–6384.

24 R. Chen, Z. Xiang, Y. Xia, Z. Ma, Q. Shi, S.-C. Wong and J. Yin, *Macromol. Rapid Commun.*, 2020, **41**, 2000206.

25 F. A. Plamper, M. Ruppel, A. Schmalz, O. Borisov, M. Ballauff and A. H. E. Müller, *Macromolecules*, 2007, **40**, 8361–8366.

26 C. Liang, X. Wang, R. Zhou, H. Shi, S. Yan, Y. Ling, S. Luan and H. Tang, *Polym. Chem.*, 2019, **10**, 2190–2202.

27 O. Bertrand, A. Vlad, R. Hoogenboom and J.-F. Gohy, *Polym. Chem.*, 2016, **7**, 1088–1095.

28 F. D. Jochum, L. zur Borg, P. J. Roth and P. Theato, *Macromolecules*, 2009, **42**, 7854–7862.

29 J. He, L. Tremblay, S. Lacelle and Y. Zhao, *Polym. Chem.*, 2014, **5**, 5403–5411.

30 J. Lee, A. J. McGrath, C. J. Hawker and B.-S. Kim, *ACS Macro Lett.*, 2016, **5**, 1391–1396.

31 C. Luo, Y. Liu and Z. Li, *Macromolecules*, 2010, **43**, 8101–8108.

32 J. Huang, X. Chen, H. Qin, H. Liang and J. Lu, *Polymer*, 2019, **160**, 99–106.

33 K. Wang, S. Chen and W. Zhang, *Macromolecules*, 2017, **50**, 4686–4698.

34 Z. Song, K. Wang, C. Gao, S. Wang and W. Zhang, *Macromolecules*, 2016, **49**, 162–171.

35 C. Zhao, Z. Ma and X. X. Zhu, *Prog. Polym. Sci.*, 2019, **90**, 269–291.

36 S. Li, H. S. Chung, A. Simakova, Z. Wang, S. Park, L. Fu, D. Cohen-Karni, S. Averick and K. Matyjaszewski, *Biomacromolecules*, 2017, **18**, 475–482.

37 F. H. Sobotta, F. Hausig, D. O. Harz, S. Hoeppener, U. S. Schubert and J. C. Brendel, *Polym. Chem.*, 2018, **9**, 1593–1602.

38 C. Fu, C. Zhang, H. Peng, F. Han, C. Baker, Y. Wu, H. Ta and A. K. Whittaker, *Macromolecules*, 2018, **51**, 5875–5882.

39 H. Batz, V. Hofmann and H. Ringsdorf, *Macromol. Chem. Phys.*, 1973, **169**, 323–325.

40 S. Li, M. Omi, F. Cartieri, D. Konkolewicz, G. Mao, H. Gao, S. E. Averick, Y. Mishina and K. Matyjaszewski, *Biomacromolecules*, 2018, **19**, 3754–3765.

41 F. El Mohtadi, R. d'Arcy, X. Yang, Z. Y. Turhan, A. Alshamsan and N. Tirelli, *Int. J. Mol. Sci.*, 2019, **20**, 4583.

42 F. El Mohtadi, R. d'Arcy and N. Tirelli, *Macromol. Rapid Commun.*, 2019, **40**, 1800699.

43 S. Perrier, *Macromolecules*, 2017, **50**, 7433–7447.

44 A. E. Smith, X. Xu and C. L. McCormick, *Prog. Polym. Sci.*, 2010, **35**, 45–93.

45 Y. Liu, J. He, J. Xu, D. Fan, W. Tang and Y. Yang, *Macromolecules*, 2005, **38**, 10332–10335.

46 Q. Zhang, C. Weber, U. S. Schubert and R. Hoogenboom, *Mater. Horiz.*, 2017, **4**, 109–116.

47 M. Kano and E. Kokufuta, *Langmuir*, 2009, **25**, 8649–8655.

48 J.-F. Lutz, *J. Polym. Sci., Part A: Polym. Chem.*, 2008, **46**, 3459–3470.

49 G. Vancoillie, D. Frank and R. Hoogenboom, *Prog. Polym. Sci.*, 2014, **39**, 1074–1095.

50 V. Aseyev, H. Tenhu and F. M. Winnik, in *Self Organized Nanostructures of Amphiphilic Block Copolymers II*, Springer, 2010, pp. 29–89.

51 L. D. Blackman, M. I. Gibson and R. K. O'Reilly, *Polym. Chem.*, 2017, **8**, 233–244.

52 K. Zhou, Y. Lu, J. Li, L. Shen, G. Zhang, Z. Xie and C. Wu, *Macromolecules*, 2008, **41**, 8927–8931.

53 M. Wadhwa, C. Bird, P. Dilger, P. Rigsby, H. Jia and M. E. B. Gross, *J. Immunol. Methods*, 2017, **447**, 14–22.

54 C. A. Chaves, C. E. Vergani, D. Thomas, A. Young, C. A. Costa, V. M. Salih and A. L. Machado, *J. Tissue Eng.*, 2014, **5**, 2041731414540911.

55 M. A. Al Enezy-Ulbrich, H. Malyaran, R. D. de Lange, N. Labude, R. Plum, S. Rütten, N. Terefenko, S. Wein, S. Neuss and A. Pich, *Adv. Funct. Mater.*, 2020, 2003528.

56 H. Otsuka, T. Hagiwara and S. Yamamoto, *J. Nanosci. Nanotechnol.*, 2014, **14**, 6764–6773.